

$GaInX_3$(X = S, Se, Te): Ultra-low thermal conductivity and excellent thermoelectric performance

Zhi-Fu Duan(段志福), Chang-Hao Ding(丁长浩), Zhong-Ke Ding(丁中科), Wei-Hua Xiao(肖威华), Fang Xie(谢芳), Nan-Nan Luo(罗南南), Jiang Zeng(曾犟), Li-Ming Tang(唐黎明), and Ke-Qiu Chen(陈克求)
Citation: Chin. Phys. B, 2024, 33 (**8**): 087302. DOI: 10.1088/1674-1056/ad47e3

What follows is a list of articles you may be interested in

Diameter-dependent ultra-high thermoelectric performance of ZnO nanowires

Yinan Nie(聂祎楠), Guihua Tang(唐桂华), Yifei Li(李一斐), Min Zhang(张敏), and Xin Zhao(赵欣)
Chin. Phys. B, 2024, 33 (**4**): 047301. DOI: 10.1088/1674-1056/ad11e5

Strong anharmonicity-assisted low lattice thermal conductivities and high thermoelectric performance in double-anion Mo_2AB_2 (A = S, Se, Te; B=Cl, Br, I) semiconductors

Haijun Liao(廖海俊), Le Huang(黄乐), Xing Xie(谢兴), Huafeng Dong(董华锋), Fugen Wu(吴福根), Zhipeng Sun(孙志鹏), and Jingbo Li(李京波)
Chin. Phys. B, 2023, 32 (**10**): 107304. DOI: 10.1088/1674-1056/ace314

Enhanced thermoelectric performance of PEDOT: PSS films via ionic liquid post-treatment

Jiaji Yang(杨家雾), Xuejing Li(李雪晶), Yanhua Jia(贾艳华), Jiang Zhang(张弓), and Qinglin Jiang(蒋庆林)
Chin. Phys. B, 2022, 31 (**2**): 027302. DOI: 10.1088/1674-1056/ac2487

Enhanced thermoelectric properties in two-dimensional monolayer Si_2BN by adsorbing halogen atoms

Cheng-Wei Wu(吴成伟), Changqing Xiang(向长青), Hengyu Yang(杨恒玉), Wu-Xing Zhou(周五星), Guofeng Xie(谢国锋), Baoli Ou(欧宝立), and Dan Wu(伍丹)
Chin. Phys. B, 2021, 30 (**3**): 037304. DOI: 10.1088/1674-1056/abd163

Strategies for optimizing the thermoelectricity of PbTe alloys

Jinze Zhai(翟近泽), Teng Wang(王腾), Hongchao Wang(王洪超), Wenbin Su(苏文斌), Xue Wang(王雪), Tingting Chen(陈婷婷), Chunlei Wang(王春雷)
Chin. Phys. B, 2018, 27 (**4**): 047306. DOI: 10.1088/1674-1056/27/4/047306

GaInX_3 (X = S, Se, Te): Ultra-low thermal conductivity and excellent thermoelectric performance

Zhi-Fu Duan(段志福)[1], Chang-Hao Ding(丁长浩)[1], Zhong-Ke Ding(丁中科)[1], Wei-Hua Xiao(肖威华)[1], Fang Xie(谢芳)[2,†], Nan-Nan Luo(罗南南)[1,‡], Jiang Zeng(曾犟)[1], Li-Ming Tang(唐黎明)[1], and Ke-Qiu Chen(陈克求)[1]

[1] *Department of Physics, School of Physics and Electronics, Hunan University, Changsha* 410082, *China*
[2] *College of Physical Science and Engineering Technology, Yichun University, Yichun* 336000, *China*

(Received 9 March 2024; revised manuscript received 2 May 2024; accepted manuscript online 7 May 2024)

Seeking intrinsically low thermal conductivity materials is a viable strategy in the pursuit of high-performance thermoelectric materials. Here, by using first-principles calculations and semiclassical Boltzmann transport theory, we systemically investigate the carrier transport and thermoelectric properties of monolayer Janus GaInX_3 (X = S, Se, Te). It is found that the lattice thermal conductivities can reach values as low as 3.07 W·m^{-1}·K^{-1}, 1.16 W·m^{-1}·K^{-1} and 0.57 W·m^{-1}·K^{-1} for $GaInS_3$, $GaInSe_3$, and $GaInTe_3$, respectively, at room temperature. This notably low thermal conductivity is attributed to strong acoustic-optical phonon coupling caused by the presence of low-frequency optical phonons in GaInX_3 materials. Furthermore, by integrating the characteristics of electronic and thermal transport, the dimensionless figure of merit ZT can reach maximum values of 0.95, 2.37, and 3.00 for $GaInS_3$, $GaInSe_3$, and $GaInTe_3$, respectively. Our results suggest that monolayer Janus GaInX_3 (X = S, Se, Te) is a promising candidate for thermoelectric and heat management applications.

Keywords: thermoelectric performance, thermal conductivity, Boltzmann transport, two-dimensional materials

PACS: 73.50.Lw, 72.15.Jf, 74.25.fc, 74.25.Kc **DOI:** 10.1088/1674-1056/ad47e3

1. Introduction

Thermoelectric (TE) materials have the potential to convert waste heat directly into electricity and can play an important role in solving global warming and the energy crises.[1–4] Seeking for high performance TE materials has been a hotspot of research. The performance of TE materials is determined by the dimensionless figure of merit ZT because it reflects the TE conversion efficiency. ZT can be expressed as

$$ZT = S^2\sigma T/(\kappa_e + \kappa_l), \tag{1}$$

where S is the Seebeck coefficient, σ is the electronic conductivity, $S^2\sigma$ is the power factor, T is the absolute temperature, and κ_e and κ_l are the electronic and lattice thermal conductivities, respectively.[5,6] Currently, the achieved ZT values of TE materials are relatively low, which strictly restricts their widespread application.[7,8] A lot of effort has been made to improve the ZT values of existing TE materials, including band engineering to improve the power factor[9–11] and phonon engineering to suppress the thermal conductivity.[12–18] However, due to the Wiedemann–Franz law,[19] to enhance ZT through band engineering is a complex issue because the power factor and the electronic thermal conductivity are complexly connected. In addition, phonon engineering methods such as hierarchical architecting and introducing defects would inevitably disturb the electronic transport.[20,21]

Searching for materials with intrinsically low lattice thermal conductivity is another avenue to obtain high TE performance materials[22,23] because this approach helps to simplify complex TE parameters and optimize TE performance. Due to their unique physical structures, low-dimensional materials possess a variety of physical properties,[24–30] which provides new possibilities for achieving low thermal conductivity and high TE performance. For instance, the material SnSe exhibits a high TE figure of merit as a result of its low thermal conductivity, while the half-Heusler compound PCdNa is noteworthy for its low thermal conductivity coupled with superior TE performance.[31,32]

Previous research has demonstrated that reducing a material's geometric symmetry can significantly reduce its thermal conductivity.[33] Vertically asymmetric Janus materials naturally have lower symmetry than their symmetric counterparts, and thus have been potential high performance TE materials. For example, the thermal conductivity and TE performance of Janus WSX (X = Se; Te), SnSSe, and MXY (M = Pd, Pt; X,Y = S, Se, Te) have been investigated.[34–37] However, the obtained ZT values in these materials are still relatively low, and thus searching for new Janus materials with a high ZT value is of significant importance.

In this work, based on the Boltzmann transport theory combined with first-principles calculations, the carrier transport and TE properties of monolayer Janus GaInX_3 (X = S, Se, Te) were investigated. The lattice thermal conductiv-

†Corresponding author. E-mail: xiefang2023@jxycu.edu.cn
‡Corresponding author. E-mail: luonn@hnu.edu.cn

© 2024 Chinese Physical Society and IOP Publishing Ltd

ity was first studied at room temperature, considering factors such as phonon group velocity, Grüneisen parameters, and scattering rates. The obtained lattice thermal conductivities for $GaInS_3$, $GaInSe_3$, and $GaInTe_3$ are 3.07 $W{\cdot}m^{-1}{\cdot}K^{-1}$, 1.16 $W{\cdot}m^{-1}{\cdot}K^{-1}$ and 0.57 $W{\cdot}m^{-1}{\cdot}K^{-1}$, respectively, which are comparable with that of the well-studied TE material SnSe (0.62 $W{\cdot}m^{-1}{\cdot}K^{-1}$).[31] This is attributed to the presence of low-frequency optical modes, which can enhance the scattering between optical and acoustic phonons, resulting in a lower thermal conductivity. Then, the electric transport properties and the figure of merit ZT were investigated. It is found that for $GaInS_3$, $GaInSe_3$, and $GaInTe_3$, the figure of merit ZT can reach maximum values as high as 0.95, 2.37, and 3.00, respectively.

2. Computational method

The quantities involved in the calculations of lattice thermal conductivity and electronic transport calculations were obtained through first-principles calculations based on density functional theory (DFT) using the Vienna *ab initio* simulation package (VASP).[38,39] The electron exchange and correlation interactions were treated with generalized gradient approximation (GGA) using the Perdew–Burke–Ernzerhof (PBE).[40] To prevent spurious interactions between the two-dimensional (2D) sheet and its periodic images along the z-direction, a vacuum space of 25 Å was introduced. The structural relaxation was performed using the conjugate gradient method until the absolute value of the Hellman–Feynman force converged to less than 0.0001 eV/Å. The integration over the Brillouin zone was conducted using a $17\times17\times1$ Monkhorst–Pack k-grid,[41] with an energy convergence criterion set to 1×10^{-8} eV. The ion–electron interaction was carried out by using the projector augmented wave method with a kinetic energy cutoff of 400 eV.[42] The HSE06 functional[43] was employed to obtain more accurate electronic transport properties. *Ab-initio* molecular dynamics (AIMD) simulations were conducted for the Janus $GaInX_3$ (X = S, Se, Te) monolayers. The simulations employed a 2 fs time step and a total time of 10 ps in the canonical ensemble at the temperature of 900 K to assess their thermodynamic stabilities.[44]

The calculation of second-order and third-order interatomic force constants (IFCs) was conducted using $5\times5\times1$ and $4\times4\times1$ supercells utilizing both the PHONOPY and Thirdorder packages, respectively.[45,46] A cut-off radius up to the 12th nearest neighbors was chosen to obtain the third-order IFCs. The calculation of thermal conductivity convergence in 2D materials is contingent upon the quadratic characteristic of the ZA branch near the Γ point.[47] To achieve a physically accurate quadratic phonon dispersion for low-frequency ZA phonons, we utilized the Hiphive program to manipulate second-order IFCs that were initially acquired through PHONOPY.[48–50] Phonon transport properties are obtained using the phonon Boltzmann transport eqnarray as implemented in ShengBTE code,[51] where a denser q-point mesh of $50\times50\times1$ is used to ensure convergence (see the supporting information for details). The κ_l is given by[51]

$$\kappa^{xy}=\frac{1}{k_{\mathrm{B}}T^2NV}\sum_{\lambda}(\hbar\omega_{\lambda})^2 f_{\lambda}^{0}\left(1+f_{\lambda}^{0}\right)v_{\lambda}^{x}F_{\lambda}^{y}, \tag{2}$$

where k_{B} is the Boltzmann constant, T is the temperature, V is the volume of the primary cell, $\hbar$ is the reduced Planck constant, ω_{λ} is the angular frequency of the phonon mode λ, N is the total number of q sampling points, and v is the group velocity of phonons. F_{λ}^{y} is the projection of the mean free path along the y direction. The electronic transport properties are obtained by solving the semiclassical Boltzmann transport eqnarray with a denser k-mesh of $35\times35\times1$ and the constant relaxation time approximation using the BoltzTraP2 software package.[52] Here, S and σ can be expressed as

$$S=-\frac{1}{eT}\frac{\sum_{n,k}(E_{nk}-E_{\mathrm{f}})v_{nk}^{2}\frac{\partial f_{nk}}{\partial E_{nk}}}{\sum_{n,k}v_{nk}^{2}\frac{\partial f_{nk}}{\partial E_{nk}}}, \tag{3}$$

$$\sigma=-\frac{e^2}{NV}\sum_{n,k}v_{nk}^{2}\tau_{\mathrm{e}}\frac{\partial f_{nk}}{\partial E_{nk}}, \tag{4}$$

where n and k are the band index and wave vectors of the electronic states, respectively. E_{nk} is the electron energy, N is the total number of k points, and v_{nk} is the group velocity. τ_{e} is the electron relaxation time, calculated through deformation potential theory within the effective mass approximation framework,[53,54] which can be determined by the subsequent eqnarray

$$\tau_{\mathrm{e}}=\frac{\mu m^{*}}{e}=\frac{2\hbar^3C}{3k_{\mathrm{B}}Tm^{*}E_1^2}, \tag{5}$$

where C, m^{*}, E_1 and k_{B} are the elastic modulus, the effective mass, the DP constant, and the Boltzmann constant, respectively. According to the Wiedemann–Franz law, κ_{e} is proportional to σ and temperature and can be expressed as

$$\kappa_{\mathrm{e}}=L\sigma T, \tag{6}$$

where L is the Lorenz number. To obtain more reliable results for κ_l, σ, and κ_{e} in 2D materials, a normalization process is conducted to compensate for the additional length introduced by the vacuum space applied along the non-periodic direction.[12,55] This normalization is achieved by the ratio of L/t, where L represents the cell length along the direction with the added vacuum, and t stands for the effective thickness of the 2D materials (see the supporting information for details).

3. Results and discussion

3.1. Structure and stability

Monolayer Janus $GaInX_3$ (X = S, Se, Te) belongs to the $R3m$ space group, as shown in Figs. 1(a) and 1(b). The optimized lattice constants for $GaInS_3$, $GaInSe_3$, and $GaInTe_3$

are 3.79 Å, 3.98 Å, and 4.24 Å, respectively, which align with the results reported in the literature.[56] They are dynamically stable because there are no imaginary frequencies in their phonon spectra, as shown in Figs. 1(c)–1(e). In addition, AIMD simulations indicate that these materials remain stable at 900 K (see the supporting information for details). As shown in Figs. 1(f)–1(h), the HSE06 functional gives similar band dispersions as the PBE functional but with an enlarged bandgap. $GaInS_3$ is a direct bandgap semiconductor with the valence band maximum (VBM) and conduction band minimum (CBM) located at the Γ point. Meanwhile, $GaInTe_3$ and $GaInSe_3$ are indirect bandgap semiconductors with their CBM and VBM located at the Γ point and along the Γ–M line. The obtained bandgap energies of $GaInS_3$, $GaInSe_3$, and $GaInTe_3$ are 1.793 eV (0.935 eV), 1.130 eV (0.415 eV), and 0.68 eV (0.147 eV), respectively by using the HSE06 (PBE) functional. The gradual decrease of the bandgaps in this series mainly comes from the decrease of the X p orbital ionization energies as X becomes heavier[57–60] (details are shown in Fig. S1 in the supporting information).

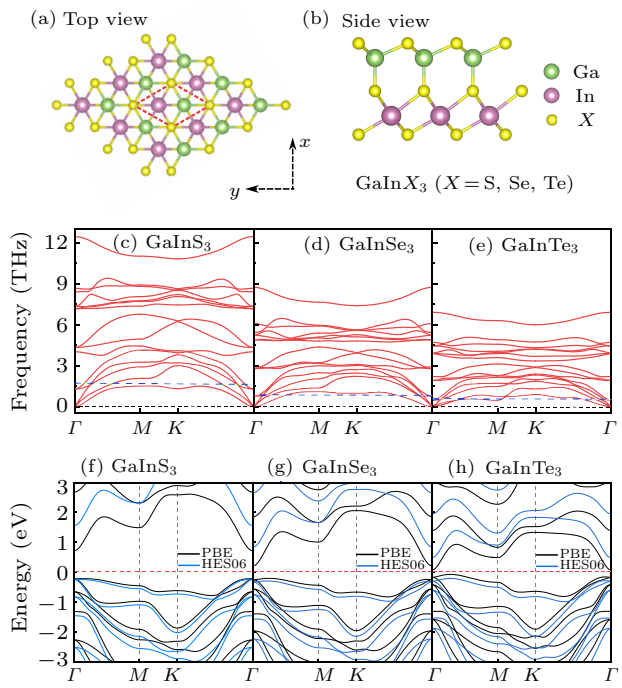


Fig. 1. Top (a) and side (b) views of the optimized $GaInX_3$ (X = S, Se, Te) monolayer structure. Phonon dispersions of $GaInS_3$ (c), $GaInSe_3$ (d), and $GaInTe_3$ (e). Band structures for $GaInS_3$ (f), $GaInSe_3$ (g), and $GaInTe_3$ (h) obtained using the PBE (black curves) and HSE06 (blue curves) functionals. The Fermi level is represented by the red dashed lines.

3.2. Thermal transport properties

Figures 1(c)–1(e) show that low-energy optical phonon modes emerge in these materials, indicating strong scattering between optical and acoustic phonons.[58,61–63] The lattice thermal conductivities (κ_l) of these materials are then investigated and the results are shown in Fig. 2(a). At 300 K, κ_l reaches values as low as 3.07 $W{\cdot}m^{-1}{\cdot}K^{-1}$, 1.16 $W{\cdot}m^{-1}{\cdot}K^{-1}$, and 0.57 $W{\cdot}m^{-1}{\cdot}K^{-1}$ for $GaInS_3$, $GaInSe_3$, and $GaInTe_3$, respectively, which are much lower than that of the well-studied monolayer MoS_2 (116.8 $W{\cdot}m^{-1}{\cdot}K^{-1}$)[64] and are comparable to those of 2D group IV–VI semiconductors, such as SnSe, SnS, GeSe, and GeS (2.2–10.5 $W{\cdot}m^{-1}{\cdot}K^{-1}$).[65] In addition, κ_l decreases with the increase of temperature. To understand the physical mechanism behind the low κ_l value obtained, the frequency-resolved phonon contributions to κ_l are investigated. Taking that obtained at 300 K as an example, it is shown that the low-frequency phonon contribution to κ_l is dominant and the accumulative κ_l achieves 80% of the total κ_l below 2.87 THz, 2.42 THz, and 2.17 THz for $GaInS_3$, $GaInSe_3$, and $GaInTe_3$, respectively, as depicted in Figs. 2(b)–2(d). Simultaneously, there is a pronounced decrease in the contribution of phonons to the thermal conductivity at frequencies of 2.24 THz, 1.1 THz, and 0.86 THz, in $GaInS_3$, $GaInSe_3$, and $GaInTe_3$, respectively. This phenomenon comes from the high phonon–phonon scattering rate, especially between TA, LA, and low frequency optical phonon branches as shown in Figs. 3(a)–3(c). This enhanced scattering effect consequently leads to a diminished contribution of acoustic phonons to the total κ_l, thereby reducing the overall thermal conductivity of the material.

From a general point of view, κ_l is primarily determined by the interactions among the harmonic and anharmonic parameters.[66–68] The former include second-order force constants, phonon group velocities, and atomic masses, and the latter mainly involve third-order force constants and three-phonon scattering processes. This makes it very complicated to reveal the physics behind the low κ_l.[69] However, it is found that κ_l is largely determined by the phonon group velocity v and the Grüneisen parameter γ ($\kappa_l \propto v^3/\gamma^2$).[70–73] v can be obtained from the phonon spectra via

$$v_\lambda(q) = \frac{\mathrm{d}\omega_\lambda(q)}{\mathrm{d}q}. \tag{7}$$

As depicted in Figs. 3(d)–3(f), the calculated maximum values of v are 4.62 km/s, 4.11 km/s, and 2.67 km/s for $GaInS_3$, $GaInSe_3$, and $GaInTe_3$, respectively, which are comparable to the well-known 2D TE materials SnSe (2.7 km/s), PtSe (3.02 km/s), and SnTe (4.0 km/s).[31,74] As X becomes heavier (from S to Te), the bond length increases and the bond strength weakens in the $GaInX_3$ series, which leads to a gradual softening of the phonon modes (Figs. 1(c)–1(e)). This gives a gradual reduction in the group velocity.[75] (see the supporting information for more details.) γ describes the anharmonic interactions of a crystal, which can be expressed as

$$\gamma_\lambda(q) = -\frac{V}{\omega_\lambda(q)}\frac{\partial\omega_\lambda(q)}{\partial V}. \tag{8}$$

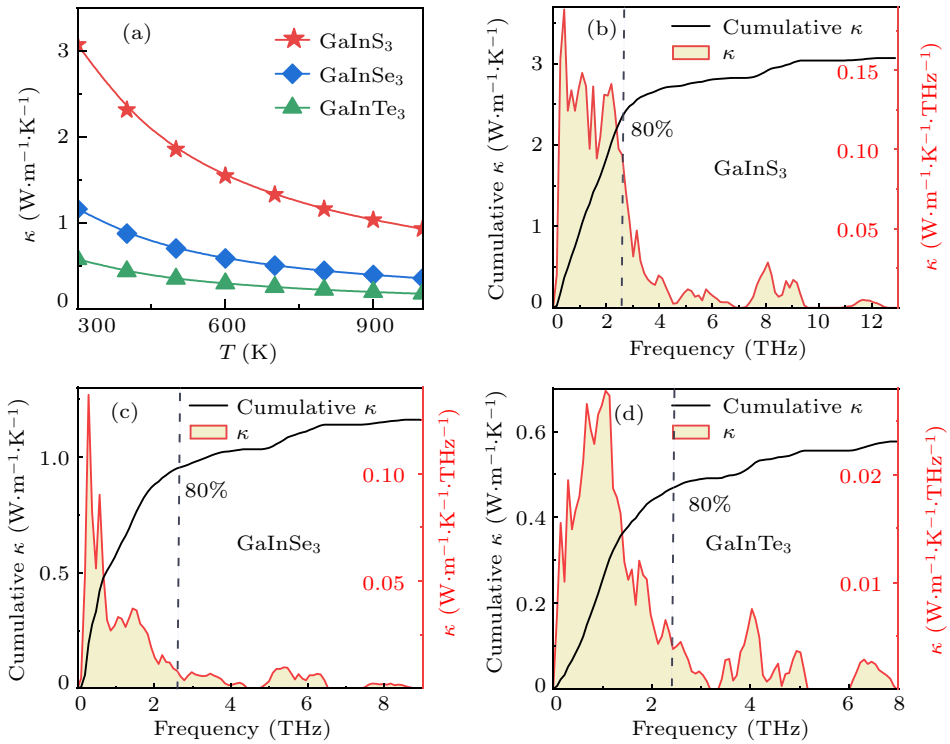


Fig. 2. (a) Lattice thermal conductivities of GaInX_3 (X = S, Se, Te) materials as a function of temperature. At 300 K, the cumulative lattice thermal conductivity (black solid line) and the frequency-dependent lattice thermal conductivity (red solid line) of $GaInS_3$ (b), $GaInSe_3$ (c), and $GaInTe_3$ (d).

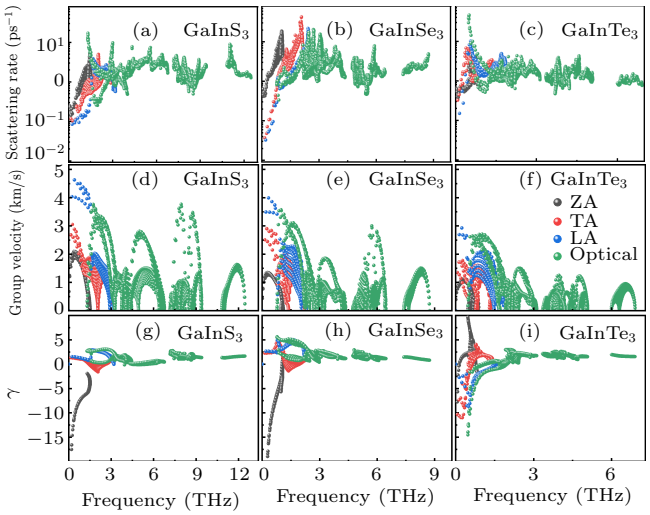


Fig. 3. The calculated three-phonon scattering rate (a)–(c), the group velocity (d)–(f), and the Grüneisen constant (g)–(i) of GaInX_3 (X = S, Se, Te) materials.

In general, systems with larger $|\gamma|$ exhibit stronger anharmonicity, resulting in higher phonon-phonon scattering rates and lower κ_l.[73] As depicted in Figs. 3(g)–3(i), the magnitude of $|\gamma|$ is considerably large in low energy phonon regions, which is comparable to that of the excellent TE materials SnSe ($|\gamma| = 2.83$) and PbTe ($|\gamma| = 1.45$).[31,61] To understand the strong anharmonicity shown in these materials, the bonding features are investigated. It is shown that nonbonding electron lone pairs[12,76,77] emerge in these materials (details are shown in the supporting information). These electron lone pairs will interact with the bonding electrons of neighboring atoms, which creates nonlinear electrostatic repulsion. This nonlinear electrostatic repulsion is the origin of the observed strong lattice anharmonicity.[21,71,78] A small v combined with a large $|\gamma|$ results in a low κ_l in these materials. In particular, v decreases from $GaInS_3$ to $GaInSe_3$ and $GaInTe_3$, while $|\gamma|$ is comparable in these materials in the low energy phonon region. This is the reason why the value of κ_l in $GaInS_3$ is the largest and in $GaInTe_3$ is the smallest.

3.3. Electronic transport and TE properties

According to Eqs. (4) and (6), the relaxation time τ is required to obtain the electrical conductivity (σ) and the electronic thermal conductivity (κ_e). Therefore, τ is first obtained based on Eq. (5) and the corresponding data are shown Table 1. It is noted that, because the band dispersions obtained using the HSE06 and the PBE functionals are similar, τ is obtained using the PBE functional to save computational efforts. It is shown that the electron has a much longer relaxation time than the hole in the three studied materials. This is mainly because the electron has a much smaller effective mass. Then, the three TE parameters S, σ and κ_e are investigated using the HSE06 functional to obtain more accurate results.

Table 1. Calculated effective mass (m^*), elastic constant (C_{2D}), deformation potential (E_1), and relaxation time (τ) for electrons (e) and holes (h) in monolayer GaInX_3 at 300 K.

Material	Carrier	C_{2D} (N/m)	m^*/m_0	E_1 (eV)	τ (ps)
$GaInS_3$	e	91	0.207	6.43	0.128
	h	91	–2.9	7.7	0.006
$GaInSe_3$	e	75	0.159	5.47	0.191
	h	75	–1.84	6.98	0.011
$GaInTe_3$	e	58	0.122	5.18	0.233
	h	58	–0.98	5.96	0.021

As shown in Figs. 4(a)–4(c), since the valence bands near the Fermi level have a flatter dispersion compared to that of the conduction bands, the density of states is larger for the valence bands.[79] Consequently, the absolute values of S ($|S|$) for p-type doping are much larger than that for n-type doping in the three studied materials within the experimentally accessible doping regime. Meanwhile, σ and κ_e have the opposite trends, as shown in Figs. 4(d)–4(i), because they are proportional to the carrier relaxation time. Specifically, for p-type doping, $|S|$ decreases with increasing carrier concentration in $GaInS_3$ and $GaInSe_3$. However, for $GaInTe_3$, $|S|$ decreases with increasing carrier concentration at 300 K and 600 K. Meanwhile, it first increases and then decreases at 900 K. This discrepancy comes from the bipolar conduction effect that the thermally excited electrons and holes in low carrier concentration system at high temperature will have a high proportion in narrow bandgap semiconductors. Since the Seebeck effects from electrons and holes have opposite signs, they cancel each other to some extent, which results in a reduced $|S|$ at elevated temperatures.[80,81] For n-type doping, the variation of S is more complicated and it tends to zero eventually as a function of carrier concentration. Meanwhile, the electrical conductivities from the thermally excited electrons and holes have the same signs, leading to an enhanced σ at low carrier concentration in p-type $GaInTe_3$ at 900 K.

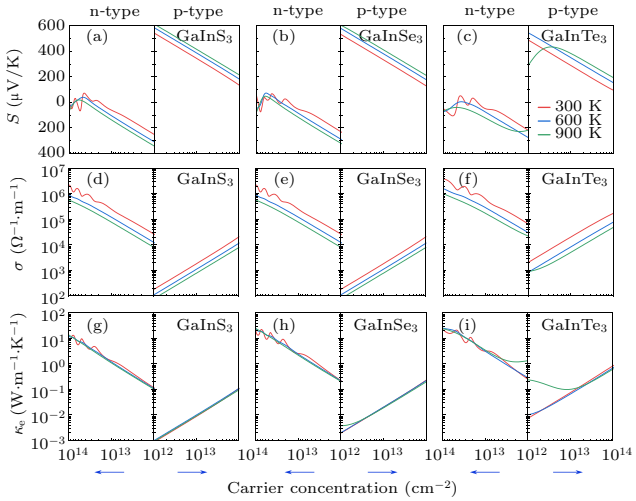


Fig. 4. The calculated Seebeck coefficient (S) (a)–(c), the electrical conductivity coefficient (σ) (d)–(f), and the electronic thermal conductivity coefficient (κ_e) (g)–(i) as a function of carrier concentration for p-type and n-type $GaInX_3$ (X = S, Se, Te) at 300 K, 600 K, and 900 K.

Table 2. The maximum ZT values for p-type and n-type $GaInS_3$, $GaInSe_3$, and $GaInTe_3$ at temperatures of 300 K, 600 K, and 900 K.

Material	Type	ZT		
		300 K	600 K	900 K
$GaInS_3$	n	0.17	0.53	0.95
	p	0.03	0.14	0.29
$GaInSe_3$	n	0.57	1.49	2.37
	p	0.20	0.62	1.15
$GaInTe_3$	n	1.13	2.36	1.43
	p	0.85	1.98	3.00

Finally, the TE performance of the three studied materials is investigated. As depicted in Fig. 5, the ZT value increases with temperature in $GaInS_3$ and $GaInSe_3$ for both n-type and p-type dopings. However, this trend breaks down in $GaInTe_3$ due to the bipolar effect. The optimal ZT values of the three materials within the experimentally accessible doping regime at 300 K, 600 K, and 900 K are shown in Table 2.

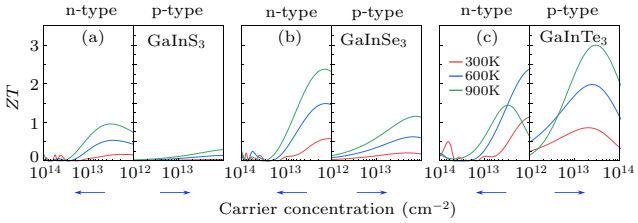


Fig. 5. The obtained ZT values of $GaInS_3$ (a), $GaInSe_3$ (b), and $GaInTe_3$ (c) as a function of carrier concentration for both n-type and p-type doping at 300 K, 600 K, and 900 K.

The TE performance of n-type doping is clearly superior to that of p-type doping for $GaInS_3$ and $GaInSe_3$ at 300 K, 600 K, and 900 K. Meanwhile, for $GaInTe_3$ n-type doping is still superior at 300 K and 600 K, but the maximum ZT value for p-type doping is larger than that of n-type doping at 900 K. The maximum ZT values for $GaInSe_3$, $GaInSe_3$, and $GaInTe_3$ are 0.95 (900 K), 2.37 (900 K), and 3.00 (900 K), respectively, which indicates that they are potential high-temperature TE materials. In addition, at 300 K, the maximum ZT value for $GaInTe_3$ is 0.85, which is notably larger than that of the well-studied SnSe (0.7).[82] This demonstrates its great potential in room-temperature TE device applications.

4. Conclusion

In conclusion, we have studied the thermal transport and TE properties of Janus $GaInX_3$ (X = S, Se, Te). The presence of low-frequency optical phonon modes leads to a high scattering rate and a large Grüneisen parameter in the low-frequency phonon region, resulting in an ultra-low lattice thermal conductivity in these materials. Furthermore, within the experimentally accessible doping regime, the electronic properties of narrow-gap semiconductors $GaInTe_3$ are significantly influenced by the bipolar effect at high temperatures, which reduces their TE performance in such conditions. At room temperature, the obtained TE figure of merit ZT can reach values as high as 0.85 in $GaInTe_3$. In addition, the maximum values of ZT are 0.95 (900 K), 2.37 (900 K), and 3.00 (900 K) for $GaInS_3$, $GaInSe_3$, and $GaInTe_3$, respectively. Our research elucidates the mechanisms behind the low thermal conductivity of $GaInX_3$ (X = S, Se, Te) materials and highlights their potential in TE and heat management applications.

Acknowledgements

Project supported by the National Natural Science Foundation of China (Grant Nos. 12104145, 62201208, and

12374040). Numerical computations were performed at the National Supercomputer Center in Changsha.

References

[1] Yang L, Chen Z G, Dargusch M S and Zou J 2018 *Advanced Energy Materials* **8** 1701797
[2] Biswas K, He J, Blum I D, Wu C I, Hogan T P, Seidman D N, Dravid V P and Kanatzidis M G 2012 *Nature* **489** 414
[3] Heremans J P, Jovovic V, Toberer E S, Saramat A, Kurosaki K, Charoenphakdee A, Yamanaka S and Snyder G J 2008 *Science* **321** 554
[4] Sootsman J R, Chung D Y and Kanatzidis M G 2009 *Angewandte Chemie International Edition* **48** 8616
[5] Bruzzone S and Fiori G 2011 *Appl. Phys. Lett.* **99** 222108
[6] Christensen M, Abrahamsen A B, Christensen N B, Juranyi F, Andersen N H, Lefmann K, Andreasson J, Bahl C R and Iversen B B 2008 *Nat. Mater.* **7** 811
[7] Chu S, Cui Y and Liu N 2017 *Nat. Mater.* **16** 16
[8] Zhao L D, Lo S H, Zhang Y, Sun H, Tan G, Uher C, Wolverton C, Dravid V P and Kanatzidis M G 2014 *Nature* **508** 373
[9] Pei Y, Wang H and Snyder G J 2012 *Adv. Mater.* **24** 6125
[10] Liu W, Tan X, Yin K, Liu H, Tang X, Shi J, Zhang Q and Uher C 2012 *Phys. Rev. Lett.* **108** 166601
[11] Jia T, Carrete J, Madsen G K, Zhang Y and Wei S H 2022 *Phys. Rev. B* **105** 245203
[12] Nissimagoudar A S, Rashid Z, Ma J and Li W 2020 *Inorganic Chemistry* **59** 14899
[13] Skoug E J and Morelli D T 2011 *Phys. Rev. Lett.* **107** 235901
[14] Jia P Z, Mo Z X, Deng L Q, Zhang Y, Yu X, Zeng Y J, Deng Y X and Xie Z X 2024 *Diamond and Related Materials* **141** 110609
[15] Poudel B, Hao Q, Ma Y, Lan Y, Minnich A, Yu B, Yan X, Wang D, Muto A, Vashaee D, *et al*. 2008 *Science* **320** 634
[16] Jiang J H, Lu S and Chen J 2023 *Chin. Phys. Lett.* **40** 096301
[17] He J, Yu C, Lu S, Zhang Z and Chen J 2024 *Appl. Phys. Lett.* **124** 022201
[18] Zeng Y J, Liu Y Y, Zhou W X and Chen K Q 2018 *Chin. Phys. B* **27** 036304
[19] Jonson M and Mahan G 1980 *Phys. Rev. B* **21** 4223
[20] Broido D A, Malorny M, Birner G, Mingo N and Stewart D A 2007 *Appl. Phys. Lett.* **91** 231922
[21] Feng Z, Jia T, Zhang J, Wang Y and Zhang Y 2017 *Phys. Rev. B* **96** 235205
[22] He J, Hu Y, Li D and Chen J 2022 *Nano Research* **15** 3804
[23] Sales B, Mandrus D and Williams R K 1996 *Science* **272** 1325
[24] Ding Z K, Zeng Y J, Pan H, Luo N, Zeng J, Tang L M and Chen K Q 2022 *Phys. Rev. B* **106** L121401
[25] He R, Wang D, Luo N, Zeng J, Chen K Q and Tang L M 2023 *Phys. Rev. Lett.* **130** 046401
[26] Pan H, Tang L M and Chen K Q 2022 *Phys. Rev. B* **105** 064401
[27] Pan H, Ding Z K, Zeng B W, Luo N N, Zeng J, Tang L M and Chen K Q 2023 *Phys. Rev. B* **107** 104303
[28] Wang Y, Luo N, Zeng J, Tang L M and Chen K Q 2023 *Phys. Rev. B* **108** 054401
[29] Ding Z K, Zeng Y J, Liu W, Tang L M and Chen K Q 2024 *Advanced Functional Materials* 2401684
[30] Liu W, Ding Z K, Luo N, Zeng J, Tang L M and Chen K Q 2024 *Phys. Rev. B* **109** 115422
[31] Xiao Y, Chang C, Pei Y, Wu D, Peng K, Zhou X, Gong S, He J, Zhang Y, Zeng Z, *et al*. 2016 *Phys. Rev. B* **94** 125203
[32] Ye X, Feng Z, Zhang Y, Zhao G and Singh D J 2022 *Phys. Rev. B* **105** 104309
[33] Yang R, Yue S, Quan Y and Liao B 2021 *Phys. Rev. B* **103** 184302
[34] Patel A, Singh D, Sonvane Y, Thakor P and Ahuja R 2020 *ACS Applied Materials & Interfaces* **12** 46212
[35] Tao W L, Lan J Q, Hu C E, Cheng Y, Zhu J and Geng H Y 2020 *J. Appl. Phys.* **127** 035101
[36] Tang S, Bai S, Wu M, Luo D, Zhang J, Wang D, Yang S and Zhao L D 2022 *Materials Today Physics* **29** 100923
[37] Geng J, Zhang P, Tang Z and Ouyang T 2024 *Chin. Phys. B* **33** 046501
[38] Kresse G and Furthmüller J 1996 *Phys. Rev. B* **54** 11169
[39] Stratmann R E, Scuseria G E and Frisch M J 1998 *The Journal of Chemical Physics* **109** 8218
[40] Perdew J P, Burke K and Ernzerhof M 1996 *Phys. Rev. Lett.* **77** 3865
[41] Monkhorst H J and Pack J D 1976 *Phys. Rev. B* **13** 5188
[42] Kresse G and Joubert D 1999 *Phys. Rev. B* **59** 1758
[43] Heyd J, Scuseria G E and Ernzerhof M 2003 *The Journal of Chemical Physics* **118** 8207
[44] Tuckerman M E, Ungar P J, Von Rosenvinge T and Klein M L 1996 *The Journal of Physical Chemistry* **100** 12878
[45] Togo A 2023 *J. Phys. Soc. Jpn.* **92** 012001
[46] Togo A, Chaput L, Tadano T and Tanaka I 2023 *J. Phys.: Condens. Matter* **35** 353001
[47] Carrete J, Li W, Lindsay L, Broido D A, Gallego L J and Mingo N 2016 *Mater. Res. Lett.* **4** 204
[48] Brorsson J, Hashemi A, Fan Z, Fransson E, Eriksson F, Ala-Nissila T, Krasheninnikov A V, Komsa H P and Erhart P 2022 *Advanced Theory and Simulations* **5** 2100217
[49] Eriksson F, Fransson E and Erhart P 2019 *Advanced Theory and Simulations* **2** 1800184
[50] Errea I, Calandra M and Mauri F 2014 *Phys. Rev. B* **89** 064302
[51] Li W, Carrete J, Katcho N A and Mingo N 2014 *Computer Physics Communications* **185** 1747
[52] Madsen G K, Carrete J and Verstraete M J 2018 *Computer Physics Communications* **231** 140
[53] Du G, Li C and Cheng L 2023 *Phys. Rev. B* **107** 085422
[54] Xiao W H, Zeng B, Ding Z K, Pan H, Liu W W, Li Q Q, Yang K, Luo N, Zeng J, Chen K Q and Tang L M 2023 *Appl. Phys. Lett.* **123** 013101
[55] Zhu X L, Liu P F, Zhang J, Zhang P, Zhou W X, Xie G and Wang B T 2019 *Nanoscale* **11** 19923
[56] Vu T V, Hieu N N, Lavrentyev A, Khyzhun O, Lanh C V, Kartamyshev A, Phuc H V and Hieu N V 2022 *RSC advances* **12** 7973
[57] Bernard J E and Zunger A 1987 *Phys. Rev. B* **36** 3199
[58] Liao H, Huang L, Xie X, Dong H, Wu F, Sun Z and Li J 2023 *Chin. Phys. B* **32** 107304
[59] Wang Q H, Kalantar-Zadeh K, Kis A, Coleman J N and Strano M S 2012 *Nat. Nanotechnol.* **7** 699
[60] Singh A K and Hennig R G 2014 *Appl. Phys. Lett.* **105** 042103
[61] Liu P F, Bo T, Xu J, Yin W, Zhang J, Wang F, Eriksson O and Wang B T 2018 *Phys. Rev. B* **98** 235426
[62] Yao H, Chen C, Cao F, Mao J, Liu X, Zhang Q and Lin X 2023 *Phys. Rev. B* **108** 195206
[63] Liu W, Xie Y, Yuan J and Chen Y 2022 *Nanoscale* **14** 8797
[64] Jin Z, Liao Q, Fang H, Liu Z, Liu W, Ding Z, Luo T and Yang N 2015 *Scientific Reports* **5** 18342
[65] Shafique A and Shin Y H 2017 *Scientific Reports* **7** 506
[66] Julian C L 1965 *Phys. Rev.* **137** A128
[67] Chang C and Zhao L D 2018 *Materials Today Physics* **4** 50
[68] Roufosse M and Klemens P 1973 *Phys. Rev. B* **7** 5379
[69] Wang H, Qin G, Li G, Wang Q and Hu M 2018 *2D Materials* **5** 015022
[70] Jia T, Liu X, Zhang Y and Wei S H 2023 *Phys. Rev. B* **107** 115204
[71] Morelli D T, Jovovic V and Heremans J P 2008 *Phys. Rev. Lett.* **101** 035901
[72] Slack G A 1973 *Journal of Physics and Chemistry of Solids* **34** 321
[73] Broido D, Ward A and Mingo N 2005 *Phys. Rev. B* **72** 014308
[74] Zhang D, Hu S, Sun Y, Liu X, Wang H, Wang H, Chen Y and Ni Y 2020 *ES Energy & Environment* **10** 59–65
[75] Chen Z, Zhang X and Pei Y 2018 *Adv. Mater.* **30** 1705617
[76] Zhou S, Liu C C, Zhao J and Yao Y 2018 *npj Quantum Materials* **3** 16
[77] Lei S, Wang X, Li B, Kang J, He Y, George A, Ge L, Gong Y, Dong P, Jin Z, *et al*. 2016 *Nat. Nanotechnol.* **11** 465
[78] Zhang L, Du M H and Singh D J 2010 *Phys. Rev. B* **81** 075117
[79] Kumar S and Schwingenschlögl U 2016 *Phys. Rev. B* **94** 035405
[80] Graziosi P, Li Z and Neophytou N 2022 *Appl. Phys. Lett.* **120** 072102
[81] Gong J, Hong A, Shuai J, Li L, Yan Z, Ren Z and Liu J M 2016 *Physical Chemistry Chemical Physics* **18** 16566
[82] Zhao L D, Tan G, Hao S, He J, Pei Y, Chi H, Wang H, Gong S, Xu H, Dravid V P, *et al*. 2016 *Science* **351** 141